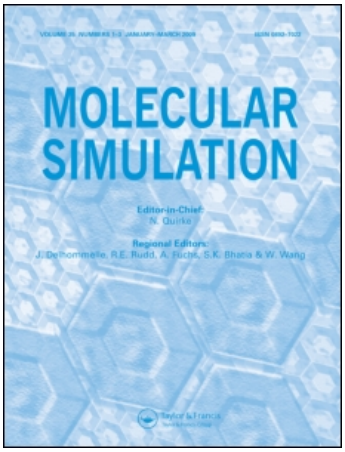

Molecular Simulation
Publication details, including instructions for authors and subscription information:
http://www.informaworld.com/smpp/title~content=t713644482

Kinetic structures in multi-phase liquid-crystalline composite materials

Susanta K. Das[a]; Alejandro D. Rey[a]
[a] Department of Chemical Engineering, McGill University, Montreal, Quebec, Canada

To cite this Article Das, Susanta K. and Rey, Alejandro D.(2005) 'Kinetic structures in multi-phase liquid-crystalline composite materials', Molecular Simulation, 31: 2, 201 — 206
To link to this Article: DOI: 10.1080/08927020412331332613
URL: http://dx.doi.org/10.1080/08927020412331332613

Molecular Simulation, Vol. 31, No. 2–3, 15 February–15 March 2005, 201–206

Kinetic structures in multi-phase liquid-crystalline composite materials

SUSANTA K. DAS and ALEJANDRO D. REY*

Department of Chemical Engineering, McGill University, 3610 University Street, Montreal, Quebec, Canada H3A 2B2

(Received April 2004; in final form November 2004)

A mesoscopic kinetic model for phase separation in the presence of liquid crystalline order has been formulated and solved using high performance numerical methods. The thermodynamic phase diagram on temperature–polymer concentration plane indicates the presence of coexistence regions between isotropic and liquid crystalline phases. These regions are partitioned by the phase-separation spinodal and the phase-ordering spinodal. We characterize the morphologies following temperature quenches in the phase diagram. The scenario is completely different from isotropic mixing since the continuous phase exhibits liquid crystalline ordering. Microdomains of the dispersed phase induce long- and short-range forces affecting the kinetics of the phase separation and the emerging structures. Presence of topological defects and elastic distortions around the microdomains formed during the phase separation dominate the morphology. The free energy of the system establishes dynamics and correlations of the morphological structures.

Keywords: Multiphase; Phase separation; Microdomain structures; Topological defects; Phase diagram

1. Introduction

Multiphase polymer–liquid crystal blends are new multifunctional materials with unique electro-optical properties. The formation process is driven by thermodynamic instabilities, and the emerging microstructures reflect the curvature elasticity of the liquid crystalline phase. Such multiphase polymer dispersed liquid crystal (PDLC) makes a new composite material with unique physical properties that originate from the orientational ordering of the liquid crystal. Mechanical and electro-optical properties of this system are primarily determined by the collective behaviors of these binary mixtures. Because when flexible polymers are introduced into the liquid crystals (LC's) the electro-optical properties of the system are considerably affected due to the deformation of the nematic director field, which can result in nontrivial collective behaviors, leading to the formation of spatially modulated structures. Depending on the time scale that controls these processes, a rich variety of morphologies have been observed [1,2]. Phase separation of such systems can be induced either through a thermal quench [3,4] or through polymerization [5]. Because of the number of nonequilibrium processes involved, however, there is a little theoretical understanding of the factors that control the domain morphology. A Cahn–Hilliard framework that allows composition and orientational density to evolve in a coupled fashion as functions of position and time following a temperature quench was performed [3]. Their framework includes the orientational density's second-order tensorial nature [6] where free energy of the system contains orientational density's three term gradient expansions.

In experimental investigations, optical microscopy during the PIPS process was used to elucidate the morphology development and to determine the phase separation dynamics in polymer–liquid crystal mixtures [4,7,8]. One significant feature in the investigation of dynamical structures of polymer–liquid crystal mixtures is the presence of topological defects during the phase transition, phase separation and pattern formation processes [2,9,10]. Topological defects are classified according to dimensionality (walls, lines, points), strength (1/2,1,...) and charge (+ or −). Oppositely (similarly) charged defects attract (repel) each other. Defect annihilations result from the coalescence of two

*Corresponding author. Tel.: +1-514-398-4196. Fax: +1-514-398-6678. E-mail: alejandro.rey@mcgill.ca

Molecular Simulation
ISSN 0892-7022 print/ISSN 1029-0435 online © 2005 Taylor & Francis Group Ltd
http://www.tandf.co.uk/journals
DOI: 10.1080/08927020412331332613

oppositely charged defects of equal strength. The topological classification of defects in liquid crystals and the corresponding topological dynamics have been verified experimentally [11,12]. When a single homogeneous phase is quenched into the biphasic (nematic–isotropic) coexistence region, due to the broken symmetry, a number of topological defects appear in the system [1]. The role of texture formation through defect nucleation in nematic phase ordering was simulated using the Landau–de Gennes nematic tensor order model [13]. But details morphological structures, especially the free energy profiles of the system, characterization of morphological structures, phase separation and phase transition mechanism, topological defect structures, etc. remain unclear yet.

In this paper, we present a non-local dynamical model focusing on the interplay between phase-separation and phase-ordering kinetics in mixtures of short, liquid crystals (rigid rods) and long, flexible polymers, as a first step towards the rational design and control of the microdomain morphology. Here, we consider fully non-local model without resorting to the three term gradient expansions of Landau-type [6] while derived free energy of the system. Computationally, this is challenging because it would require evaluating multiple convolutions at each moment in time. The advantage of our system is that we can calculate two order parameters (conserved and non-conserved) solving two coupled time-dependent equations together from a microscopic model of polymers and liquid crystals without loosing any information of order parameters.

2. Model formulation

2.1 Thermodynamic phase diagram

In this section, we represent the free energy to construct the static phase diagrams. According to Ref. [14], the free energy density of polymer–liquid crystal mixtures can be written as;

$$f(\varphi, S) = \beta \Delta F_{\text{mix}}/N_T = f^{(i)} + f^{(n)}, \tag{1}$$

$$f^{(i)} = \frac{\varphi_{\text{I}}}{n_{\text{I}}} \ln \varphi_{\text{I}} + \frac{\varphi_{\text{A}}}{n_{\text{A}}} \ln \varphi_{\text{A}} + \chi \varphi_{\text{I}} \varphi_{\text{A}}, \tag{2}$$

$$f^{(n)} = \frac{1}{2}\left(\frac{\Gamma_0}{n_{\text{A}}}\right)\varphi_{\text{A}}^2 S^2 - \frac{\varphi_{\text{A}}}{n_{\text{A}}} \ln\left(\frac{I_0(\Gamma_0 \varphi_{\text{A}} S)}{2}\right), \tag{3}$$

$$\varphi_{\text{I}} + \varphi_{\text{A}} = 1, \quad \Gamma_0 = (\chi_{\text{a}} + 5/4)n_{\text{A}}, \quad \beta = 1/k_{\text{b}}T, \tag{4}$$

$$I_0 = (\Gamma_0 \varphi_{\text{A}} S) = \int_{-1}^{1} \exp\left(\frac{3}{2}\Gamma_0 \varphi_{\text{A}} S\left(x^2 - \frac{1}{3}\right)\right) \mathrm{d}x, \tag{5}$$

where T is the absolute temperature, k_{b} is the Boltzmann constant, S is the "scalar" orientational order parameter of the liquid crystals, χ is the Flory–Huggin's interaction parameter [15], the terms and χ_{a} and $(5/4)n_{\text{A}}$ in Γ_0 indicates the orientation-dependent attractive interactions [16] between the mesogens and excluded volume interactions [17] between mesogenic molecules, respectively, n_{I} and n_{A} are the number of segments on the isotropic (monomer or polymer) component and the number of segments (axial ratios) on the mesogen, respectively, and ϕ_{I} and ϕ_{A} are the corresponding volume fractions, respectively. The first two terms in the right hand side of equation (2) represent the entropy of mixing. For thermodynamical reasons, the entropy of mixing must be dominant at high temperatures and so we can introduce the temperature parameter, τ, defined by $1/\tau = \chi = U_0/k_{\text{b}}T$, where U_0 controls the miscibility of the two species in the isotropic phase. The two terms on the right side of equation (3) represent the free energy change due to the alignment of the liquid crystals.

As shown by De Gennes and Prost [6] equations (1–5) predict the emergence of a stable nematic phase when $\Gamma_0 \varphi_{\text{A}} = 4.55$. Using the following definitions:

$$\Gamma_0 = (\chi_{\text{a}} + 5/4)n_{\text{A}}, \quad \alpha = \chi_{\text{a}}/\chi, \quad \chi = 1/\tau, \tag{6}$$

where $\alpha = \chi_{\text{a}}/\chi$ represents the relative strength of interactions, and τ is the reduced temperature, it is found that the threshold $\Gamma_0 \varphi_{\text{A}} = 4.55$ gives the following concentration dependence of the reduced nematic-isotropic transition (NIT) temperature:

$$\tau_{\text{NI}}(\varphi_{\text{A}}) = \frac{\alpha n_{\text{A}} \varphi_{\text{A}}}{4.55 - 1.25 n_{\text{A}} \varphi_{\text{A}}}. \tag{7}$$

For simplicity, we denote the isotropic component composition, ϕ_1, by $\phi(\phi \equiv \phi_{\text{I}})$ in the phase diagram (figure 1).

3. Kinetic equations

The dimensionless total free energy of the system consists of the bulk free energy and a non-local free energy that controls the cost of gradients in composition and orientational density, in the absence of surface terms and external fields, can be expressed as [18]

$$\tilde{F} = \tilde{T} \oint_{\tilde{v}} \left(\tilde{f}^h + \frac{1}{\tilde{T}}\tilde{f}^g\right) \mathrm{d}\tilde{v}, \tag{8}$$

$$\tilde{f}^h = \left[\frac{\phi}{n_{\text{I}}} \ln \phi + \frac{(1-\phi)}{n_{\text{A}}} \ln(1-\phi) + \chi\phi(1-\phi) + \frac{3}{4}\left(\frac{\tilde{I}_0}{n_{\text{A}}}\right)(1-\phi)^2 \tilde{Q} : \tilde{Q} - \frac{(1-\phi)}{n_{\text{A}}} \ln\left(\frac{\tilde{I}_0}{2}\right)\right], \tag{9}$$

$$\tilde{f}^g = \left[\frac{1}{2\tilde{D}}(\tilde{\nabla}\phi)^2 + \frac{\tilde{R}}{\tilde{D}}\left(\tilde{\partial}_i \phi\right)\left(\tilde{\partial}_j \tilde{Q}_{ij}\right) + \frac{\tilde{G}}{2\tilde{D}}\left(\tilde{\partial}_k \tilde{Q}_{ij}\right)^2 + \frac{\tilde{P}}{2\tilde{D}}\left(\tilde{\partial}_i \tilde{Q}_{ik}\right)\left(\tilde{\partial} \tilde{Q}_{jk}\right)\right], \tag{10}$$

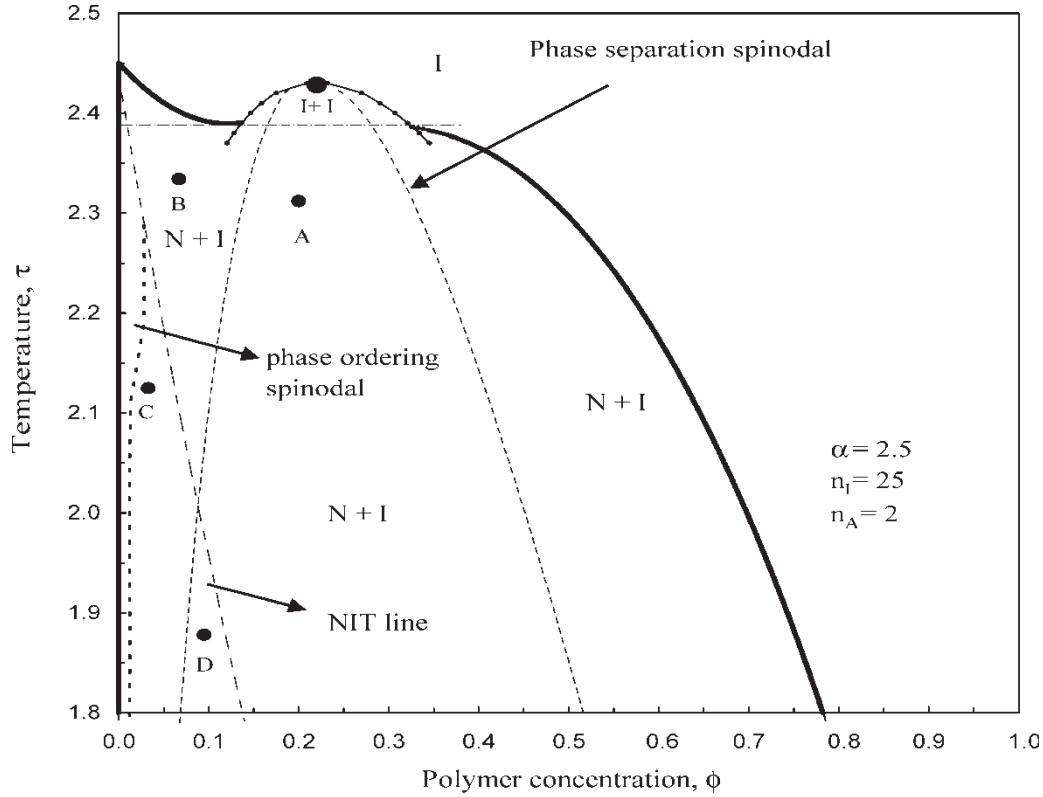

Figure 1. Phase diagram of the system on the temperature-concentration plane computed with $n_{\mathrm{I}} = 25$, $n_{\mathrm{A}} = 2$, and $\alpha = 2.5$.

where

$$\tilde{I}_0 = \int_0^{2\pi}\int_0^{\pi} \exp\left[\frac{3}{2}\tilde{\Gamma}_0(1-\phi)\tilde{\mathbf{Q}} : \left(\sigma\sigma - \frac{\boldsymbol{\delta}}{3}\right)\right] \sin^2\theta \,\mathrm{d}\theta\,\mathrm{d}\omega. \tag{11}$$

The dimensionless governing kinetic equations of the system becomes [18]

$$\frac{\partial\phi}{\partial\tilde{t}} = \left[\tilde{D}\tilde{\Gamma}\tilde{\nabla}^2\left(\frac{\partial\tilde{f}^h}{\partial\phi}\right) - \tilde{\nabla}^4\phi - \tilde{R}\tilde{\nabla}^2\left(\tilde{\nabla}\cdot\tilde{\nabla}\tilde{\mathbf{Q}}\right)\right], \tag{12}$$

$$\left[\frac{\partial\tilde{\mathbf{Q}}}{\partial\tilde{t}}\right]^{[s]} = \left[-\tilde{T}\tilde{D}\tilde{E}\frac{\partial\tilde{f}^h}{\partial\tilde{\mathbf{Q}}} + \tilde{E}\tilde{R}\tilde{\nabla}\cdot\tilde{\nabla}\phi + \tilde{E}\tilde{G}\tilde{\nabla}^2\tilde{\mathbf{Q}} + \tilde{E}\tilde{P}\tilde{\nabla}\left(\nabla\cdot\tilde{\mathbf{Q}}\right)\right]^{[s]}, \tag{13}$$

where $\tilde{t}$ is the dimensionless time, $\tilde{D}$ is the dimensionless diffusion parameter, $\tilde{E}$ is the phenomenological constant, $\tilde{R}$ is the coupling parameter, $\tilde{G}$, and $\tilde{P}$ represents dimensionless Frank elastic parameters [19], respectively, and $\tilde{\mathbf{Q}}$ is a second rank symmetric and traceless tensor [6,13].

4. Numerical methods

We simulate incompressible mixtures of flexible polymers made up of $n_{\mathrm{I}} = 25$ monomers and low molar mass rod-like mesogens (liquid crystals with $n_{\mathrm{A}} = 2$ monomers). The governing dimensionless set of partial differential equations (12), (13) is transformed into a set of ordinary differential equations by spatial discretization using second-order centered finite difference approximations. Time integration is performed with a stabilized explicit Runge-Kutta–Chebyshev adaptive time integration algorithm [20]. The governing equation for the conserved parameter, ϕ, is a non-linear parabolic partial differential equation, while the governing equation for $\mathbf{Q}$ is a set of five coupled, time-dependent, non-linear, partial integro-differential equations. Mesh and time step independence was established. The computational domain is the unit square ($0 \le \tilde{x} \le 1, 0 \le \tilde{y} \le 1$) discretized into 4096 cells. All integrations were performed using the composite Simson's rule [21] with sufficient accuracy.

The auxiliary data for equations (12), (13) consist of two initial conditions and thirty-six periodic boundary conditions. The initial conditions were taken in the form of the isotropic uniform mixtures with small random fluctuations. The initial conserved parameter is obtained as:

$$\phi_0 = \phi|_{\mathrm{ini}} + \varepsilon_0(\tilde{x}, \tilde{y}, \tilde{t} = 0), \tag{14}$$

where $\phi|_{\mathrm{ini}}$ is the initial polymer concentration and ε_0 is a Gaussian noise representing infinitesimal fluctuations. The initial tensor order parameter field $\mathbf{Q}_0 = \mathbf{Q}_0(\tilde{x}, \tilde{y}, \tilde{t} = 0)$ is

$$\mathbf{Q}_0 = S_0\left(\mathbf{n}_0\mathbf{n}_0 - \frac{\boldsymbol{\delta}}{3}\right), \tag{15}$$

where the initial director field, $\mathbf{n}_0$, is a random unit vector and the initial scalar order parameter, S_0, is a Gaussian noise representing infinitesimal fluctuations. The boundary

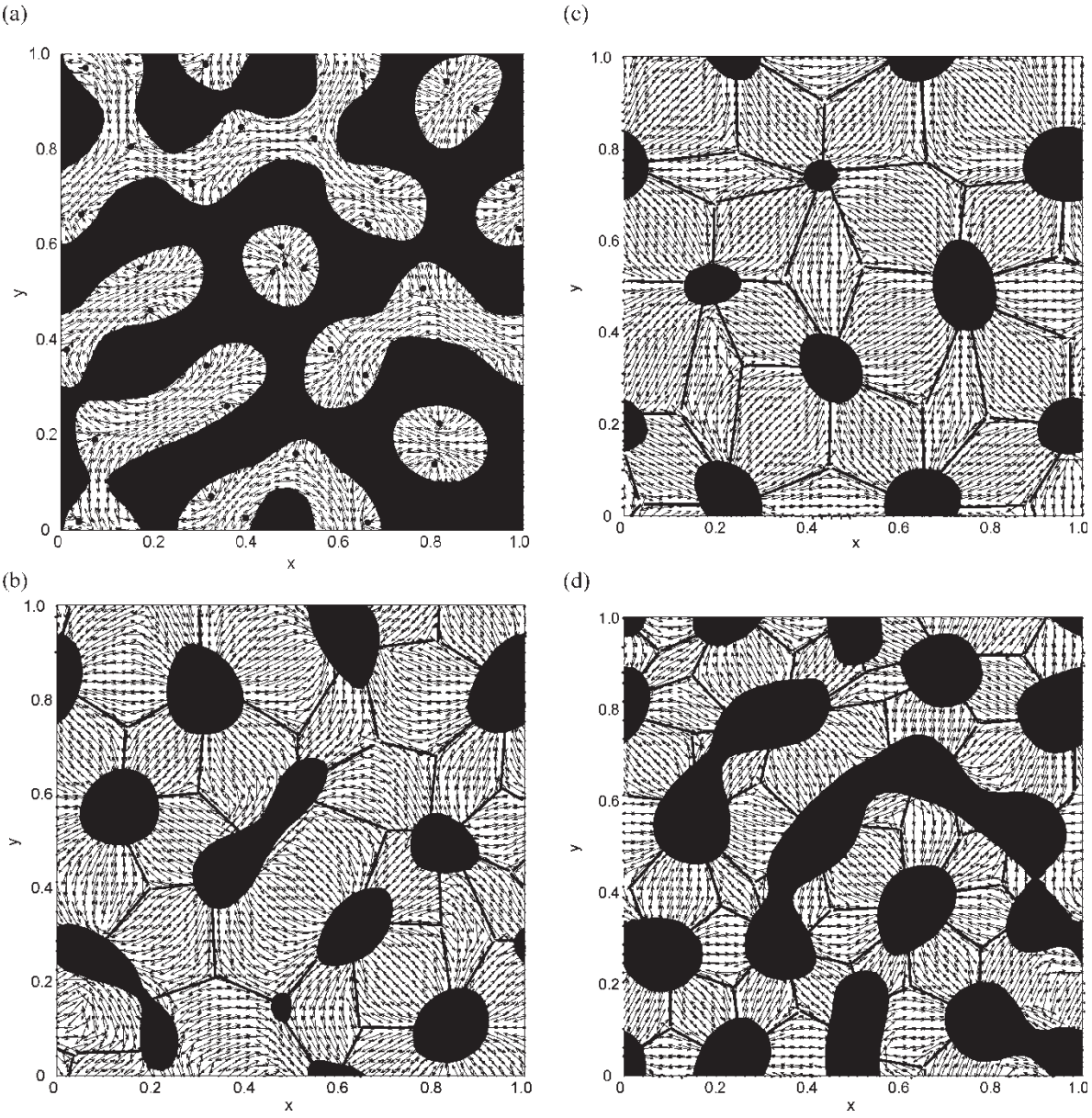

Figure 2. Snapshot of the local composition of the system at a late time step following a quench to; (a) point A, (b) point B, (c) point C and (d) point D for $n_I = 25$, $n_A = 2$, $\alpha = 2.5$, $\tilde{D} = 1000$, $\tilde{E} = 1.0$, $\tilde{R} = 0.2$, $\tilde{G} = 0.1$, and $\tilde{P} = 0.1$. Black corresponds to isotropic polymer and white corresponds to pure liquid crystals (LCs). The arrows represent the local nematic director, and defects are marked with small solid circles.

conditions are periodic in both the $\tilde{x}$- and $\tilde{y}$-directions:

$$\phi(\tilde{x}=0) = \phi(\tilde{x}=1), \quad \phi(\tilde{y}=0) = \phi(\tilde{y}=1), \tag{16}$$

$$\mathbf{Q}(\tilde{x}=0) = \mathbf{Q}(\tilde{x}=1), \quad \mathbf{Q}(\tilde{y}=0) = \mathbf{Q}(\tilde{y}=1), \tag{17}$$

$$\left.\frac{\partial^m \phi}{\partial \tilde{x}^m}\right|_{\tilde{x}=0} = \left.\frac{\partial^m \phi}{\partial \tilde{x}^m}\right|_{\tilde{x}=1}, \left.\frac{\partial^n \phi}{\partial \tilde{y}^n}\right|_{\tilde{y}=0} = \left.\frac{\partial^n \phi}{\partial \tilde{y}^n}\right|_{\tilde{y}=1}, \tag{18}$$

$$\left.\frac{\partial^{m+n} \phi}{\partial \tilde{x}^m \partial \tilde{y}^n}\right|_{\tilde{x}=0} = \left.\frac{\partial^{m+n} \phi}{\partial \tilde{x}^m \partial \tilde{y}^n}\right|_{\tilde{x}=1}, \left.\frac{\partial^{m+n} \phi}{\partial \tilde{x}^m \partial \tilde{y}^n}\right|_{\tilde{y}=0} = \left.\frac{\partial^{m+n} \phi}{\partial \tilde{x}^m \partial \tilde{y}^n}\right|_{\tilde{y}=1}, \tag{19}$$

$$\left.\frac{\partial^m \mathbf{Q}}{\partial \tilde{x}^m}\right|_{\tilde{x}=0} = \left.\frac{\partial^m \mathbf{Q}}{\partial \tilde{x}^m}\right|_{\tilde{x}=1}, \left.\frac{\partial^n \mathbf{Q}}{\partial \tilde{y}^n}\right|_{\tilde{y}=0} = \left.\frac{\partial^n \mathbf{Q}}{\partial \tilde{y}^n}\right|_{\tilde{y}=1}, \tag{20}$$

where $n = 1, 2, 3$; and $m = 1, 2, 3$ and $m + n \leq 3$. For simplicity in the results section, due to presentation reasons, we used $x(x = \tilde{x})$ and $y(y = \tilde{y})$ instead of $\tilde{x}$ and $\tilde{y}$ respectively.

In our model, there are five dimensionless parameters related to coefficients of gradient terms of S and ϕ, and three adjustable parameters related to the thermodynamic phase diagram. These parameters may be obtained by extending the mean field theory [16] for liquid crystalline polymers to binary mixtures of nematogens. Here, we set $n_I = 25$, $n_A = 2$, $\alpha = 2.5$, $\tilde{D} = 1000$, $\tilde{E} = 1.0$, $\tilde{R} = 0.2$, $\tilde{G} = 0.1$, and $\tilde{P} = 0.1$ for all the calculation performed at each of the quenching points.

5. Results and discussions

A typical phase diagram of the system on the temperature-concentration plane is shown in figure 1, which is computed with $n_I = 25$, $n_A = 2$, and $\alpha = 2.5$. In the fgiure, ϕ, denotes the isotropic component composition (polymer concentration). The coexistence (binodal) curve of the phase equilibrium is derived by a double tangent method. A detailed procedure for computing binodal and spinodal curves for such a system is documented in the work [14]. We study the morphology following four quenches from the isotropic, homogeneous phase into the isotropic–nematic (IN) coexistence region below the triple point line. Four regions are indicated by filled circles and denoted by points A, B, C and D, respectively, in the phase diagram (figure 1).

Figure 2 represents the snapshot of compositional order of the system at points A, B, C and D, respectively. In figure 2(a), mass matrix phase is isotropic and droplet phase is nematic. In figure 2(a) we can see that a pair of topological defects forms inside each microdomain due to the presence of repulsive Peach–Koehler forces. In our system the repulsive force naturally arises from interaction via the elastic deformation of liquid crystal [1]. We can see from the figure 2(a) that orientation inside the droplet is perpendicular implying strong normal anchoring of liquid crystal molecules at the droplet boundary. Nematic droplets must develop defects because the LCs wants to be parallel to each other and parallel to the droplet interface too. This result agrees quite well with the results reported by Lapena *et al.* [3] (see figure 3, [3]) and Hamm *et al.* [22]. In figures 2(b)–(d), mass matrix phase is nematic and microdomain phase is isotropic. In figures 2(b)–(d), isotropic microdomains suspended into the nematic matrix are surrounded by the topological defects. One interesting feature of the defect lattice is its topology. Solid lines represent the interconnection between defect cores and isotropic microdomains. Defect structures form cellular polygonal networks that are mostly four-sided and the side of each polygon ends either at the droplet or at another defect. Most of the defects are $+1/2$ disclinations. Some of them are $+1$ disclinations that eventually split into two $+1/2$ disclinations as can be seen from figures 2(b)–(c). In the case of point C (see figure 2(c)), microdomians are almost positionally ordered whilst they form fibrillar networks for the case of point D (see figure 2(d)).

To get better understanding of underlying physics in phase separation processes, we calculated free energy profiles at each of the quenching positions of the system. Figure 3 represents the dimensionless homogeneous and gradient energy as a function of dimensionless time following quenches to the point A, B, C and D. In figure 3, we can clearly see three distinct regimes, namely initial time lag regime (I), growth/relaxation regime (II) and the plateau regime (III). In the II regime, the free energy

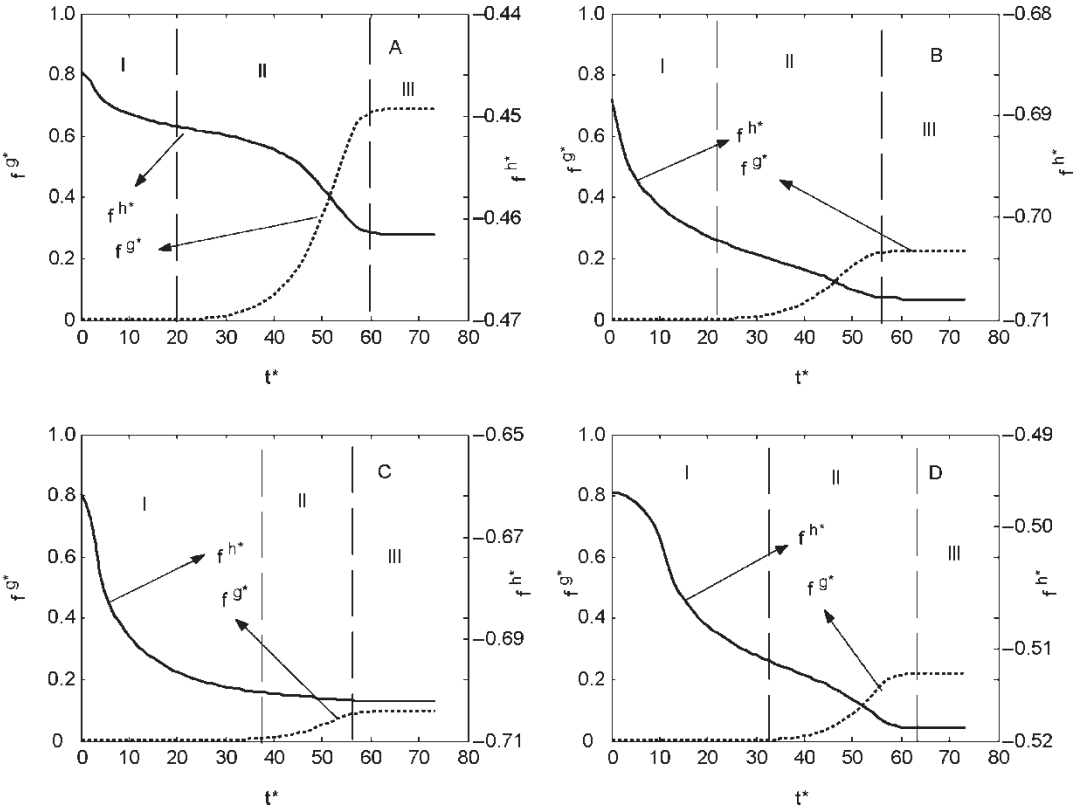

Figure 3. Free energy profiles of the system following a quench to; (a) point A, (b) point B, (c) point C and (d) point D for $n_I = 25$, $n_A = 2$, $\alpha = 2.5$, $\tilde{D} = 1000$, $\tilde{E} = 1.0$, $\tilde{R} = 0.2$, $\tilde{G} = 0.1$, and $\tilde{P} = 0.1$. Dimensionless homogeneous energy, $f^{h^*} = \tilde{T} \times \tilde{f}^h$, dimensionless gradient energy, $f^{g^*} = 325 \times \tilde{f}^g$, and dimensionless time, $t^* = 10^5 \times \tilde{t}$.

shows growth in the gradient energy and decrease in homogeneous energy indicating that phase separation and phase ordering spinodal decomposition (SD) drives the system to be unstable, leading to the breakdown of the interconnected domains and formation of isotropic microdomains or fibrillar networks. In the crossover regime III, a plateau regime corresponding to the onset of the breakdown of the interconnected structure (see figure 2) appears. The plateau is quite pronounced in both of the energy profiles, which indicates that phase separation get saturated and signals a transition from early stage to intermediate stage of phase separation.

6. Conclusions

A non-local mesoscopic dynamic model for multiple phase separation, based on a tensor theory, in the presence of liquid crystalline order has been formulated, and solved using high-performance numerical methods. We characterized the emerging morphologies following four temperatures quenches into the physically meaningful regions of the phase diagram. Phase separations from temperature quenches of isotropic binary mixtures start with the formation of small domains that grow and coarsen as time elapses which leads to polydisperse dispersions of growing microdomains that eventually phase separate macroscopically. It has been found that ordering dramatically affects morphology. Topological defects arise due to the elastic distortions around the microdomains formed during the phase separation. Defect structures form cellular polygonal networks that are mostly four-sided and the side of each polygon ends either at the droplet or at another defect. The free energy of the system establishes the dynamics and correlation of the morphological structures. Formation of interconnected (bicontinuous) networks or microdomains depends on whether ordering or phase separation is the initially dominant. process. Compared to the experimental and numerical results available in the literature, our simulation results may able to provide new insights into the understanding of new emerging microdomain topological defect morphology in liquid crystalline materials.

Acknowledgements

This work was supported in part by the Air Force Office of Scientific Research, Mathematical and Space Science Program, under grant number F49620-00-1-0341. This work was also supported in part by the ERC Program of the National Science Foundation under Award Number EEC-9731680.

References

[1] J.W. Doane. *Liquid Crystals: Applications and Uses*, B. Bahadur (Ed.), World Scientific, NJ (1990).
[2] P.S. Drzaic. *Liquid Crystal Dispersions*, World Scientific, Singapore (1995).
[3] A.M. Lapena, S.C. Glotzer, S.A. Langer, A.J. Liu. Effect of ordering on Spinodal decomposition of liquid-crystal/polymer mixtures. *Phys Rev E*, **60**(1), R29 (1999).
[4] M. Graca, S.A. Wieczorek, R. Holyst. Growth of polystyrene domains in isotropic, nematic and smectic phase of 8CB liquid crystal. *Macromolecules*, **36**, 6691–6913 (2003).
[5] G.P. Crawford, S. Zumer. *Liquid Crystals in Complex Geometries Formed by Polymer and Porous Networks*, Taylor & Francis, London (1996).
[6] P.G. de Gennes, J. Prost. *The Physics of Liquid Crystals*, Oxford University Press, NY (1993).
[7] A.J. Liu, G.H. Fredrickson. Phase separation kinetics of rod/coil mixtures. *Macromolecules*, **29**, 800–8009 (1996).
[8] A.J. Liu, G.H. Fredrickson. Free energy functionals for semiflexible polymer solutions and blends. *Macromolecules*, **26**, 2817 (1983).
[9] E.M. Terentjev. Disclination loops, standing alone and around solid particles in nematic liquid crystals. *Phys Rev E*, **51**(2), 1330 (1995).
[10] C.B. Muratov, E. Weinan. Theory of phase separation kinetics in polymer-liquid crystal systems. *J Chem Phys*, **116**(11), 4723 (2002).
[11] G.E. Volovik, O.D. Lavrentovich. Topological dynamics of defects: boojums in nematic drops. *Sov Phys JETP*, **58**, 1159 (1983).
[12] M.V. Kurik, O.D. Lavrentovich. Defects in liquid crystals: linear and point peculiarities in nematics. *Sov Phys Usp*, **31**, 196 (1988).
[13] A.D. Rey, T. Tsuji. Long range order in sheared liquid crystalline materials. *Macromol Theory Simul*, **7**, 623–639 (1998).
[14] S.K. Das, A.D. Rey. Computational modelling of multi-phase equilibria of mesogenic mixtures. *J Comp Mat Sci*, **29**, 152–164 (2004).
[15] P.J. Flory. *Principles of Polymer Chemistry*, Cornell University, Ithaca (1953).
[16] W. Maier, A. Saupe. A simple molecular theory of the nematic crystalline-liquid state. *Z Naturforsch A*, **13a**, 564–566 (1958).
[17] L. Onsager. The effects of shape on the interaction of colloidal particles. *Ann NY Acad Sci*, **51**, 627 (1949).
[18] S.K. Das, A.D. Rey. Texture formation under phase ordering and phase separation in polymer-liquid crystal mixtures. *J Chem Phys*, **121**, xxxx (2004) in press.
[19] F.C. Frank. On the theory of liquid crystals. *Discuss Faraday Soc*, **25**, 1 (1958).
[20] P.J. Van der Houwen. The development of Runge-Kutta methods for partial differential equations. *Appl Numer Math*, **20**(2), 261 (1996).
[21] A.W. Al-Khafaji, J.R. Tooley. *Numerical Methods in Engineering Practice*, The Dryden Press, Saunders College Publishing, London (1986).
[22] M. Hamm, G. Goldbeck-Wood, A.V. Zvelindovsky, J.G.E.M. Fraaije. Microstructure of nematic amorphous block copolymers: Dependence on the nematic volume fraction. *J Chem Phys*, **118**(20), 9401 (2003).